Magazine of Civil Engineering

ISSN 2712-8172

journal homepage: http://engstroy.spbstu.ru/

Research article

UDC 624.042

DOI: 10.34910/MCE.141.5

Videogrammetric method for measuring of concrete beam deformations under dynamic vertical loading

S.A.S. Sabir ✉, ***J.A.A. Al-Baghdadi, R.M. Hamdoon***

Surveying Engineering, Technical Engineering College, Baghdad, Iraq

✉ *sanaohasan4@gmail.com*

Keywords: videogrammetry, 3D coordinates, vertical loading, concrete beam, deformation, PhotoModeler software

Abstract. Many studies have examined their use in civil and close-range applications, including building structural monitoring due to advances in videogrammetric systems. However, the videogrammetric system's ability to reliably identify concrete beam dynamic deformations under vertical loads has not been fully studied. This study aims to examine the efficacy of the videogrammetric system in detecting the dynamic deformation of various concrete beams through the utilization of the videogrammetry technique. The researchers utilized PhotoModeler software to generate a three-dimensional stereo model of concrete beams. This was done both before and after applying a vertical load. The primary objective of this research is to determine the deflection values exhibited by these beams. The videogrammetric system employs a pair of stationary video cameras to record the dynamic deformations of loaded beams. This study involves the selection and calibration of two identical model video cameras, specifically the Canon IXUS. In the practical trials, three distinct types of concrete beam sections of identical length are employed. The beams possess cross-sectional dimensions of 10×13×300 cm and have been chosen with varying compositions. In the laboratory setting, the apparatus is utilized to apply a consistent load to each of the three beams. The video results are subsequently examined based on the civil design calculations. The study provides evidence that the utilization of videogrammetric system approaches enables accurate and efficient measurement of deformation in various types of concrete beams, achieving precision at the millimeter level. Based on the aforementioned findings, it is evident that this particular technique holds the potential for effective implementation and utilization in the context of conducting destructive inspections on critical civil structural components

Citation: Sabir, S.A.S., Al-Baghdadi, J.A.A., Hamdoon, R.M. Videogrammetric method for measuring of concrete beam deformations under dynamic vertical loading. Magazine of Civil Engineering. 2026. 19(1). Article. No. 14105. DOI: 10.34910/MCE.141.5

1. Introduction

Extensive investigations have been conducted in recent years about the deformation of structural elements in civil engineering. Nevertheless, the measurement of structural deformation in the bulk of these studies was conducted using conventional equipment, such as a dial gauge. Several of these equipment items are characterized by high costs, whereas the remaining one lacks precision and is not specifically engineered for measuring or displaying dynamic deformation [1]. An excellent method for assessing the performance of a structure is to measure its displacement when subjected to operational loads. Nevertheless, measuring structural deformation with high precision is still challenging, especially in complicated structures [2]. The fatigue life of the structure can be reduced by fluctuating cyclic loading. Cracks are frequently observed as a result of fatigue failure in reinforced concrete structures [3]. Various imaging techniques, including laser scanners and digital photogrammetry, have demonstrated their

effectiveness and accuracy in capturing deformations in both large and small areas subjected to static loading circumstances. Close-range photogrammetry (CRP) is widely recognised as a cost-effective, secure, and precise measuring method across various industries [4]. Videogrammetry is the technique used to acquire three-dimensional data of objects. It utilizes cameras to capture and analyse spatial data [5]. Videogrammetry, which involves determining the coordinates of object points using several video streams captured by camcorders, is an auspicious area of research that holds the capacity to surmount the constraints of current methodologies. A videogrammetric approach is automated and may produce high-quality results without the need for human intervention [6]. Recently, some studies have utilized a video camera and employed videogrammetry, a specialized branch of photogrammetry, to quantify the displacement of the oscillating bridge structure. Lidar has numerous advantages and a diverse range of applications in comparison to photogrammetry, particularly in accurately capturing the movements of objects in motion. The presence of objects makes it a desirable option as a 3D measurement tool [7, 8]. Multiple studies have suggested the potential of utilizing cameras and photogrammetric techniques to accurately quantify the movement of objects that can change shape in three dimensions [9–11]. For instance, the utilization of a high-resolution camcorder in digital photogrammetry on a shipyard enables the measurement of object points. This is done by using retro-reflective targets to provide accurate dimension checking and control [10]. To achieve precise calibration, a robust network geometry was established by capturing 8 images from 5 camera stations, some of which involved panning or rotating the camera axis [12]. Demonstrated that CRP may be employed in both static and dynamic modes. Furthermore, it emphasized the advantages of rapid measurements, comprehensive coverage, and non-contact, which were not possible with alternative methods. The researchers employed two Pulnix (TM-1020-15) digital cameras. Video cameras are used throughout the practical examinations. The cameras were fitted with a built-in ring lamp to provide uniform illumination for retroreflective targets. Moreover, numerous prior research has employed videogrammetric methods in industrial settings. A videogrammetric system with a large field of view, consisting of four cameras, was utilized to perform feature detection and matching, reconstruction of 3D coordinates and displacements, as well as computation of motion parameters. The experiments provided evidence that the suggested method achieved a high level of accuracy, with measurements of dynamic length accurate to within a margin of 0.5 mm [11].

The experiments tests showed that the four-camera video measurement system can accurately predict the position within a range of vision measuring 5000×5000 mm. Consequently, numerous researchers have successfully employed digital photogrammetric approaches to monitor deformations in structures and civil construction [13, 14]. In general, the digital photogrammetric method involves employing digital stereo images captured by a digital camera to monitor deflections in structures and civil elements. Digital photogrammetry offers numerous advantages compared to traditional tools when it comes to measuring deflection. Photogrammetry is a non-contact method that eliminates the need for manually reading dials and generates three-dimensional data. It takes measurements and generates visual recordings of the tests. It is particularly well-suited for conducting destructive testing since only a few inexpensive targets are lost or damaged, in contrast to the expensive Linear Variable Differential Transformers (LVDTs) or dial gauges [13]. For instance [15], photogrammetric techniques were used to evaluate various civil engineering materials. Two cameras with mirrors were used to analyse structures from a rear perspective. Additionally, photogrammetry was employed for on-site monitoring during load tests. Two distinct cameras were employed to capture images, and the results were compared toLVDTs displacement measures [16]. This study investigates the outcomes of utilizing photogrammetry to assess the distortions of bar and plate components in the steel structures of hoisting machines. It analyses the primary difficulties that arise during the processing of these components and suggests remedies to attain the necessary accuracy. The study suggested by [17] presents a novel videogrammetry technique to accurately measure the displacement of a vibration pre-stressed concrete bridge. The technique is applied in both daylight and day-night circumstances utilizing reflective targets. The investigation was carried out in two stages using four High-Definition (HD) video cameras. Additionally, [1] developed a unique transducer to measure the deformation of a high-speed shaking table. This was achieved by utilizing videogrammetric measurements with a high-speed CMOS camera. This study aimed to assess the precision of the shaking table's three-dimensional coordinates using the high-speed videogrammetric measurement method outlined. Based on the literature study, it is evident that digital photogrammetric and videogrammetric approaches are suitable for measuring and observing the changes in shape or structure in civil constructions. Previous studies have not examined the capability of utilizing the videogrammetric systems to identify deflections and the deformations in various types of steel beams subjected to the same load. Therefore, this study seeks to investigate the videogrammetric system's ability to detect deflections and deformations in different sections of steel beams under a dynamic uniform vertical load.

1.1. Mathematical Algorithm

The mathematical algorithm employed in videogrammetry encompasses the utilization of photogrammetric procedures, such as bundle correction, which relies on collinearity Equations (1) and (2).

Bundle adjustment is a prevalent optimization technique that finds extensive application in the field of image processing.

Scene reconstruction is a fundamental aspect of computer vision and computer graphics [18]. The methodology involves the utilization of recorded picture coordinates as well as the consideration of external and internal factors. The intrinsic camera parameters, along with the object space coordinates of the seen points, are essential components in computer vision and image processing. The latter entities exert control over the resultant nonlinear system. The equations of collinearity serve as the fundamental basis for the proposed mathematical model and integrate the observed picture coordinates with the outside and internal camera parameters. The characteristics, as well as the object space coordinates, of the observed points were determined:

$$\left(x-x_0\right)=-f+\frac{r_{11}\left(X-XL\right)+r_{21}\left(Y-YL\right)+r_{31}\left(Z-ZL\right)}{r_{13}\left(X-XL\right)+r_{23}\left(Y-YL\right)+r_{33}\left(Z-ZL\right)}; \tag{1}$$

$$\left(y-y_0\right)=-f+\frac{r_{12}\left(X-XL\right)+r_{22}\left(Y-YL\right)+r_{32}\left(Z-ZL\right)}{r_{13}\left(X-XL\right)+r_{23}\left(Y-YL\right)+r_{33}\left(Z-ZL\right)}, \tag{2}$$

where $\left(x,y\right)$, $\left(x_0,y_0\right)$: are image coordinates of an object and a principal point respectively; $\left(r_n\right)$: rotation matrix according to angles $\left(\omega,\varphi,\kappa\right)$; $\left(f\right)$: focal length of a camera; $\left(X,Y,Z\right)$, $\left(XL,YL,ZL\right)$: are ground coordinates of the object and principal point respectively.

1.2. Structural Concrete Beam Design

Three identical concrete beams were prepared and monitored for testing under emotional load. The length of the beams is 3200 mm and has a rectangular cross-section of 130×100 mm (Fig. 1a). Each type of concrete consists of a different ratio of mixtures, as the first specimen contains a mixture (1:2:4), which means one part of resistant cement two parts of fine sand and four parts of coarse gravel. The second specimen is the mixing ratio (1:3:6) one part of resistant cement, half a part of fine sand, and three parts of crushed gravel (crushed kashi). The third specimen is the mixing ratio (1:1:2), which is one part of resistant cement, one part of fine sand, and two parts of coarse gravel. The concrete used in the beams contains compressive design strength at 28 days and has a fair face. Note that the reason behind testing three concrete beams made from three different ratios of mixture is to make sure that the developed videogrammetric system can capture dynamic deformations of various types of concrete beams. Each girder is reinforced with two lower bars with a diameter of 12 mm and two top bars with a diameter of 12 (Fig. 1). Models have been tested on a testing machine.

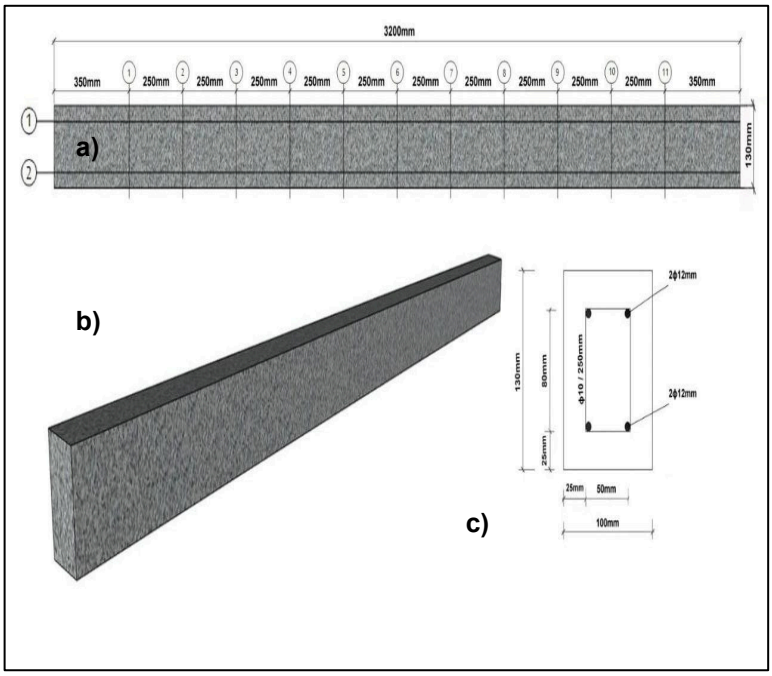

Figure 1. The tested concrete beam: a) longitudinal view; b) perspective view; c) cross-section.

2. Methods

Two non-metric Canon IXUS 185 cameras were used in the study. Additionally, engineering testing equipment manufacture was studied. The equipment is a 10-ton hydraulic jack. Three different concrete formulations have been used to make 10×13×300 cm concrete beams. Custom-made Light Emitting Diode (LED) gadget for video-frame synchronisation was used. The Topcon Total Station (GM 50 series) is used in surveying and construction. Our research relies on this equipment's exact three-dimensional ground coordinate and distance readings. The target was encoded in 10 pixels. Project management software creates targets. Print and attach captured objects. During processing, the project management software may recognise and detect targets in object photos. These targets' proportions depend on the camera's distance from captured items. This study attaches targets to industrial videogrammetric systems. These targets are likewise mounted on the systems' front of concrete beams' surfaces. Internet-accessible Virtual Dub software is free. This tool software breaks a movie into image sequences for many uses. Extract photos from the video. Software like PhotoModeler Scanner (PMS) creates precise 3D models from photos. This programme was integrated by Canadian business Eos Systems Inc. PMS has many uses. Many photogrammetric and videogrammetric applications include quantifying 3D points and creating 3D models. Using images or videos to analyse surfaces as shown in Fig. 2.

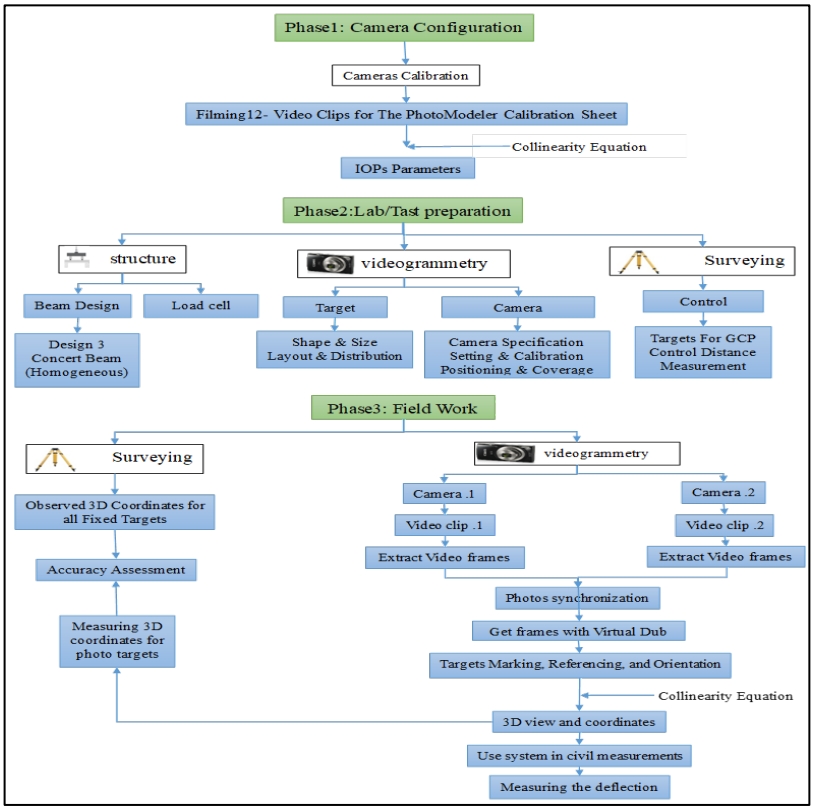

Figure 2. The chart showing the Research Methodology processing.

2.1. Video Camera Calibration

Through camera calibration, the focal length (f), main point coordinates (x_c, y_c) and radial and decentering lens distortions are determined to determine the camera's internal orientation parameters (IOPs). As [13] stated, camera characteristics largely affect relative photogrammetric measurements. The (IOPs) are calculated by linearizing collinearity equations for unknown parameters such as camera lens centre coordinates (XL, YL, ZL), orientation $(\omega, \varphi, \kappa)$, and lens distortion (K_1, K_2, K_3). K_1 provides intermediate precision. Wide-angle cameras and accurate photogrammetric applications require K_2 and K_3. Also, least-squares methods are used to determine the decentering parameters (P_1, P_2) and their affinity and shear properties (C_1, C_2). Iterative computation estimates small constant corrections like the sensor chip's principle distance (f) and principal point (x_0, y_0). The collinearity models determine the target's 3D coordinates after obtaining parameter values. The calibration sheet has four coded targets and 96 grid dots (Fig. 2a). Each camera captured 12 videos. Each camera was photographed on Fig. 3a's

calibration sheet. For calibration, each photo was taken from a different location and angle (Fig. 3b). The calibrating process for sheets frequently requires three movies from each corner. Capture video frames with Virtual Dub. The PMS programme then generates a report with the selected cameras' calibrated inner orientation parameters and camera calibration residuals Root Mean Square Error (RMSE). Information is in Table 1. Camera 1 had 0.102 pixels residuals and camera 2 0.112 pixels. Every calibration residual was below half a pixel. The lens distortion PMS calibration process has been employed to enhance the accuracy of picture coordinates. The study's camera parameters are Type (1) and type (2) cameras including the Canon IXUS 185.

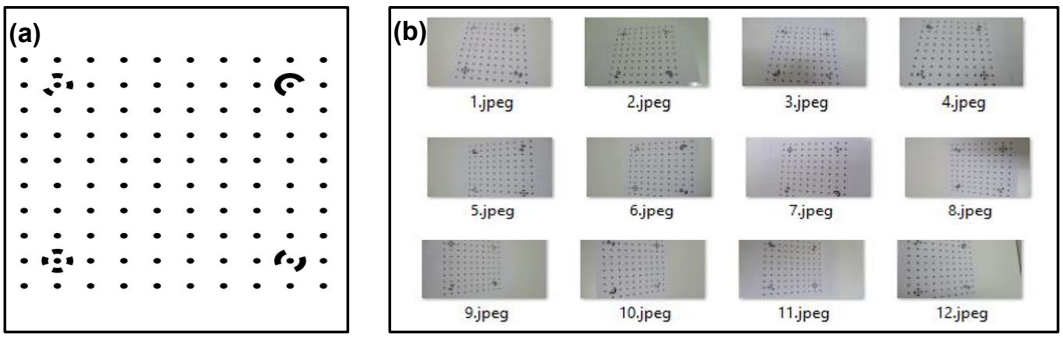

Figure 3. (a) Single-sheet for camera calibration PhotoModeler User Manual, 2020; (b) Twelve photos by every chosen camera were captured on the calibration sheet, PhotoModeler User Manual, 2020.

Table 1. Camera calibration parameters of the two selected cameras.

Items	Camera Canon IXUS 185	
	Left camera	Right Camera
Focal length	7.51563 mm	7.493389 mm
(X0, Y0)	4.596474 mm × 2.596654 mm	4.503162 mm ×2.585972 mm
K1	4.735e-04	5.540e-04
K2	–2.907e-06	–6.138e-06
K3	0.000e+00	0.000e+00
P1	–3.9843e-04	–1.971e-04
P2	3.984e-04	1.372e-04
No. of photos	12	12
Overall RMSE	o.106	0.111
Maximum RMSE	0.322	0.266

2.2. Load Cell Calibration

A load cell is a measuring instrument utilized for the direct or indirect measurement of loads. There are different types of load cells available, namely hydraulic load cells, pneumatic load cells, and strain gauge load cells [19, 20]. Only pneumatic load cells were utilized in this paper. The steel beams were attached to an electrical indication device to measure the imposed load. The calibration was performed between the load cell and the indication. By utilizing varying weights of 5 kg, 10 kg, and 15 kg, as depicted in Fig. 4.

Figure 4. Load Cell Calibration steps.

2.3. Capturing and Processing Videos

After calibration, cameras are set at the right distance from objects. To generate perfect stereo films, the base-to-height ratio was about 1. As shown in Fig. 6, "base" is the horizontal distance between the two cameras' exposure stations, while "height" is the vertical distance between the cameras, the ground, and the subject taken by the camera. As mentioned, stereo recordings use two cameras along the same line to film objects simultaneously. The video parts were then analysed and manipulated on a computer. Uploading videos to Virtual Dub turned them into frames. The two contemporaneous stereo images from the left and right cameras were visually selected for processing. The PMS determines the tridimensional (x, y, and z) coordinates of test apparatus points. Fig. 6 shows the camera's position relative to the test apparatus's targets.

Figure 6. Study area and the equipment for this investigation.

2.4. Accuracy Assessment

This article employed an accuracy assessment to validate the outcomes of video measuring methodologies. The evaluation was conducted by examining the coordinates and extracting the horizontal distances between the points; where these points were fixed on the steel frame (yellow frame), as shown in Fig. 6. The technique involves recording the coordinates of 24 targets, with 12 points serving as a control and 12 points as a chick point. A total station (GM50) with an accuracy of 1 mm was utilized to find the precise 3D ground coordinates of the 24 target points. PMS software was used also to determine the 3D ground coordinates of the 12 checkpoints using the selected stereo images from the video frames. The accuracy assessment process was done by comparing the coordinates of the 12 checkpoints that were measured using the total station with the coordinates of the same points computed using PMS. Subsequently, the variance for each point was computed, followed by the calculation of the cumulative residual of all the points.

2.5. Determining the Target Points' Three-D Coordinates for Deflection Detection

To detect deflection, the team will put 11 10-pixel targets on reinforced concrete beams. To synchronise the camera, an LED light was attached to the steel frame (Fig. 10) before videotaping. TOPCON Total Station (GM50) accuracy (1 mm) The target points' 3D ground coordinates were measured before and after loading. Video measurement determined the target points' 3D positions. Thus, the two cameras recorded six videos of the thing. The video camera's detection is tested. Load-induced deflection of three similar reinforced concrete beams with varied mixture percentages The photos' stereo recordings were uploaded from both cameras before and after the application was installed to the PC for processing. Virtual Dub converted stereo. Videos for every situation in stereo frames. Optical synchronisation of stereo frames from left and right cameras allows PMS software to calculate target point 3D coordinates. Installed encrypted targets (fixed objects) were control points. 12 checkpoints (CPs) were established to provide data tracking and calculating coordinates for targets on steel frames and concrete beams under stresses.. Ensure the 3D coordinates are precise and free of artefacts.

Figure 8. Shows the distribution targets on the test device.

3. Results and Discussion

3.1. Accuracy Assessment Result

Important (error-free) 3D coordinates of target sites as measured using a total station were considered in section 6. The device used PMS to determine the 3D spatial placement of target points attached to the steel frame using stereo video images. The 3D spatial location of target points (PMS) findings were measured by the total station, as shown in Table 2.

Table 2. 3D GCP coordinates of fixed-on-a-steel-frame targets, measured, computed, and residuals.

No.	Observed (m) (Total Station)			Computed coordinates (with photo modeller) (m)			Differences between coordinates (m)		
	x	y	z	x	y	z	vx	vy	vz
1	104.6454	101.9679	30.9364	104.6414	101.9628	30.936	0.004	0.005	0.004
2	104.4009	102.2072	30.9474	104.4059	102.2134	30.9486	–0.005	–0.006	–0.001
3	104.1327	102.4848	30.9436	104.1355	102.4876	30.9416	–0.002	–0.002	0.002
4	103.8176	102.8082	30.9429	103.8189	102.8052	30.9427	–0.001	0.003	0.002
5	103.6078	103.0228	30.9389	103.6028	103.0178	30.9387	0.005	–0.005	–0.004
6	102.9734	103.6647	30.9374	102.9722	103.6632	30.9376	0.001	0.001	–0.002
7	102.7611	103.8751	30.9279	102.7639	103.8765	30.9268	–0.002	–0.001	0.001
8	102.4655	104.1763	30.9354	102.4645	104.175	30.9366	0.001	0.001	–0.001
9	102.2094	104.4314	30.9481	102.2078	104.4298	30.9473	0.002	0.002	–0.002
10	101.9559	104.689	30.9273	101.9492	104.6855	30.9275	–0.006	0.003	–0.002
11	101.7376	104.9028	31.0787	101.7361	104.9031	31.0747	0.001	–0.003	0.004
12	103.3112	103.3678	32.0807	103.3117	103.3648	32.0787	–0.005	0.003	0.003
RMSE							0.00313	0.00321	0.00258

$$RMSE = \sqrt{\frac{\sum v2}{n}}.$$

3.2. Concrete Beam Deflection Results According to Applying Load

Three experiments were performed for each type of reinforced concrete beam of 3.2 m length utilizing a video imaging technology system to record two clips. 11 points for each type of concrete beam were determined using the four loading case weights. Tables following exhibit the length law in Equation (3) used to compute the lengths between every two coordinates of the same object point of no-load situation. According to load, these distances are concrete beam deviation values. At beam number one, the deviation value was high, notably in the bearing zone, as illustrated in Tables 3 and 4 and in Fig. 8. The concrete beam's natural high deflection, especially in the loading area, makes the video measurement system reliable for precise applications. Fig. 9 shows that the gradient in the deflection value of the second and third beams, which have significant resistance, decreases with concrete beam stiffness, verifying these readings. According to Table 5, the video imaging technology system's accuracy lies in sensing deflection values detected for small values (millimetres) and not in loading areas. Figs. 10–12 depict Tables 6 to 12.

$$L = \sqrt{(x_1 - x_2)^2 + (y_1 - y_2)^2 + (z_1 - z_2)^2}. \quad (3)$$

Table 3. The three-dimensional coordinates of the targets that were installed on the first concrete beam were measured before and after loading 300 kg.

Point	Before loading (Zero Load)			After loading (300 Kg)			Deflection (m)
	X_0 (m)	Y_0 (m)	Z_0 (m)	X_A (m)	Y_A (m)	Z_A (m)	
1	104.3971	102.3046	31.52695	104.3951	102.2966	31.51895	0.008
2	104.19	102.5238	31.52496	104.185	102.5168	31.51596	0.009
3	103.9855	102.7428	31.52421	103.9765	102.7358	31.51321	0.011
4	103.7807	102.9602	31.52325	103.7717	102.9522	31.51125	0.012
5	103.5734	103.1759	31.52564	103.5634	103.1669	31.51264	0.013
6	103.3636	103.3947	31.5255	103.3506	103.3867	31.5105	0.015
7	103.1502	103.6098	31.52291	103.1402	103.6008	31.50991	0.013
8	102.9399	103.82	31.52311	102.9309	103.812	31.51111	0.012
9	102.7266	104.0337	31.52465	102.7186	104.0277	31.51465	0.01
10	102.5201	104.2485	31.52768	102.5151	104.2415	31.51868	0.009
11	102.3093	104.4604	31.51998	102.3073	104.4524	31.51198	0.008

Table 4. The three-dimensional coordinates of the targets that were installed on the first concrete beam were measured before and after loading 600 kg.

Point	Before loading (Zero Load)			After loading (600 Kg)			Deflection (m)
	X_0 (m)	Y_0 (m)	Z_0 (m)	X_A (m)	Y_A (m)	Z_A (m)	
1	104.3971	102.3046	31.52695	104.3831	102.2956	31.50995	0.017
2	104.19	102.5238	31.52496	104.173	102.5148	31.50596	0.019
3	103.9855	102.7428	31.52421	103.9655	102.7358	31.50321	0.021
4	103.7807	102.9602	31.52325	103.7587	102.9532	31.50025	0.023
5	103.5734	103.1759	31.52564	103.5504	103.1689	31.50164	0.024
6	103.3636	103.3947	31.5255	103.3396	103.3867	31.5005	0.025
7	103.1502	103.6098	31.52291	103.1282	103.6018	31.49991	0.023
8	102.9399	103.82	31.52311	102.9189	103.813	31.50111	0.022
9	102.7266	104.0337	31.52465	102.7066	104.0297	31.50465	0.02
10	102.5201	104.2485	31.52768	102.5031	104.2395	31.50868	0.019
11	102.3093	104.4604	31.51998	102.2953	104.4514	31.50298	0.017

Table 5. The three-dimensional coordinates of the targets that were installed on the first concrete beam were measured before and after loading 900 kg.

Point	Before loading (Zero Load)			After loading (900 Kg)			Deflection (m)
	X_0 (m)	Y_0 (m)	Z_0 (m)	X_A (m)	Y_A (m)	Z_A (m)	
1	104.3971	102.3046	31.52695	104.3761	102.2876	31.49995	0.027
2	104.19	102.5238	31.52496	104.174	102.5008	31.49696	0.028
3	103.9855	102.7428	31.52421	103.9635	102.7218	31.49421	0.03
4	103.7807	102.9602	31.52325	103.7567	102.9392	31.49125	0.032
5	103.5734	103.1759	31.52564	103.5454	103.1559	31.49164	0.034
6	103.3636	103.3947	31.5255	103.3346	103.3727	31.4895	0.036
7	103.1502	103.6098	31.52291	103.1292	103.5838	31.48991	0.033
8	102.9399	103.82	31.52311	102.9169	103.799	31.49211	0.031
9	102.7266	104.0337	31.52465	102.7036	104.0127	31.49365	0.031
10	102.5201	104.2485	31.52768	102.5001	104.2275	31.49868	0.029
11	102.3093	104.4604	31.51998	102.2883	104.4434	31.49298	0.027

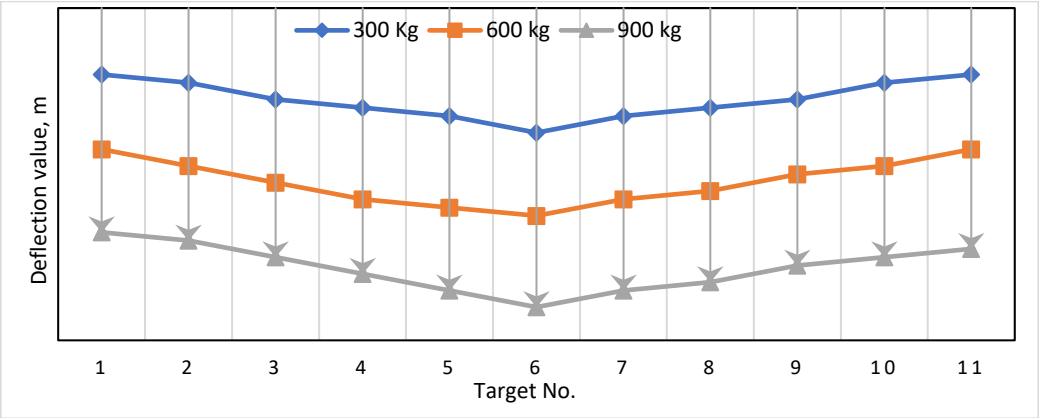

Figure 9. Beam1 deflection under 300, 600, and 900 kg vertical load.

Table 6. The three-dimensional coordinates of the targets that were installed on the second concrete beam were measured before and after loading 300 kg.

Point	Before loading (Zero Load)			After loading (300 kg)			Deflection (m)
	X_0 (m)	Y_0 (m)	Z_0 (m)	X_A (m)	Y_A (m)	Z_A (m)	
1	104.3973	102.3037	31.527	104.3953	102.2977	31.521	0.006
2	104.191	102.5241	31.5238	104.189	102.5161	31.5158	0.008
3	103.9853	102.7429	31.5232	103.9802	102.7359	31.5142	0.009
4	103.7827	102.9622	31.5228	103.7747	102.9562	31.5128	0.01
5	103.5721	103.1734	31.5263	103.5630	103.1664	31.5153	0.011
6	103.363	103.3924	31.5237	103.3520	103.3834	31.5107	0.013
7	103.153	103.6116	31.5212	103.1440	103.6036	31.5092	0.012
8	102.942	103.8199	31.5233	102.9339	103.8139	31.5133	0.01
9	102.7308	104.0351	31.5244	102.7257	104.0281	31.5154	0.009
10	102.5204	104.2475	31.5285	102.5183	104.2395	31.5205	0.008
11	102.3125	104.4628	31.5210	102.3104	104.4558	31.5140	0.007

Table 7. The three-dimensional coordinates of the targets that were installed on the second concrete beam were measured before and after loading 600 kg.

Point	Before loading (Zero Load)			After loading (600 kg)			Deflection (m)
	X_0 (m)	Y_0 (m)	Z_0 (m)	X_A (m)	Y_A (m)	Z_A (m)	
1	104.3973	102.3037	31.527	104.3833	102.2947	31.51	0.017
2	104.191	102.5241	31.5238	104.175	102.5151	31.5058	0.018
3	103.9853	102.7429	31.5232	103.968278	102.6529	31.5042	0.019
4	103.7827	102.9622	31.5228	103.762706	102.9582	31.5028	0.02
5	103.5721	103.1734	31.5263	103.552083	103.1664	31.5053	0.021
6	103.363	103.3924	31.5237	103.342019	103.3844	31.5017	0.022
7	103.153	103.6116	31.5212	103.133028	103.6046	31.5002	0.021
8	102.942	103.8199	31.5233	102.924993	103.8109	31.50433	0.019
9	102.7308	104.0351	31.5244	102.716768	104.026	31.5074	0.017
10	102.5204	104.2475	31.5285	102.507374	104.2375	31.5125	0.016
11	102.3125	104.4628	31.5210	102.299452	104.4548	31.5060	0.015

Table 8. The three-dimensional coordinates of the targets that were installed on the second concrete beam were measured before and after loading 900 kg.

Point	Before loading (Zero Load)			After loading (900 kg)			Deflection (m)
	X_0 (m)	Y_0 (m)	Z_0 (m)	X_A (m)	Y_A (m)	Z_A (m)	
1	104.3973	102.3037	31.527	104.3773	102.2967	31.506	0.021
2	104.191	102.5241	31.5238	104.17	102.5161	31.5018	0.022
3	103.9853	102.7429	31.5232	103.9632	102.7349	31.5002	0.023
4	103.7827	102.9622	31.5228	103.7587	102.9542	31.4978	0.025
5	103.5721	103.1734	31.5263	103.5510	103.1564	31.4993	0.027
6	103.363	103.3924	31.5237	103.3550	103.3654	31.4957	0.028
7	103.153	103.6116	31.5212	103.1320	103.5946	31.4942	0.027
8	102.942	103.8199	31.5233	102.9389	103.7939	31.4973	0.026
9	102.7308	104.0351	31.5244	102.7067	104.027	31.4994	0.025
10	102.5204	104.2475	31.5285	102.4973	104.2395	31.5045	0.024
11	102.3125	104.4628	31.5210	102.2914	104.454	31.4990	0.022

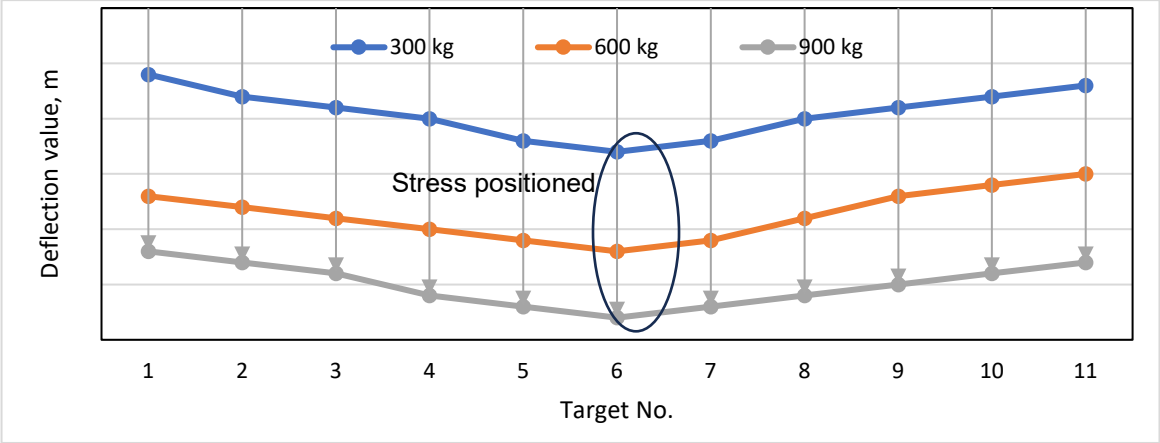

Figure 10. Beam2 deflection under 300 kg ,600 kg, and 900 kg vertical load.

Table 9. The three-dimensional coordinates of the targets that were installed on the third concrete beams were measured before and after loading 300 kg.

Point	Before loading (Zero Load)			After loading (300 kg)			Deflection (m)
	X_0 (m)	Y_0 (m)	Z_0 (m)	X_A (m)	Y_A (m)	Z_A (m)	
1	104.4011	102.324	31.533	104.3991	102.32	31.529	0.004
2	104.2012	102.557	31.527	104.1992	102.551	31.521	0.006
3	103.99	102.779	31.522	103.988	102.771	31.514	0.008
4	103.7927	102.994	31.522	103.7877	102.987	31.513	0.009
5	103.588	103.209	31.527	103.579	103.202	31.516	0.011
6	103.463	103.413	31.5247	103.454	103.405	31.5127	0.012
7	103.155	103.62	31.5213	103.146	103.613	31.5103	0.011
8	102.942	103.833	31.5273	102.934	103.827	31.5173	0.01
9	102.7408	104.052	31.53	102.7358	104.045	31.521	0.009
10	102.5402	104.267	31.531	102.5382	104.259	31.523	0.008
11	102.321	104.478	31.522	102.319	104.471	31.515	0.007

Table 10. The three-dimensional coordinates of the targets that were installed on the third concrete beam were measured before and after loading 600 kg.

Point	Before loading (Zero Load)			After loading (600 kg)			Deflection (m)
	X_0 (m)	Y_0 (m)	Z_0 (m)	X_A (m)	Y_A(m)	Z_A (m)	
1	104.4011	102.324	31.533	104.3921	102.316	31.521	0.012
2	104.2012	102.557	31.527	104.1902	102.548	31.514	0.013
3	103.99	102.779	31.522	103.977	102.771	31.507	0.015
4	103.7927	102.994	31.522	103.7787	102.985	31.505	0.017
5	103.588	103.209	31.527	103.572	103.2	31.509	0.018
6	103.463	103.413	31.5247	103.443	103.409	31.5047	0.020
7	103.155	103.62	31.5213	103.138	103.611	31.5023	0.019
8	102.942	103.833	31.5273	102.926	103.824	31.5093	0.018
9	102.7408	104.052	31.53	102.7278	104.042	31.514	0.016
10	102.5402	104.267	31.531	102.5272	104.259	31.516	0.015
11	102.321	104.478	31.522	102.31	104.469	31.509	0.013

Table 11. The three-dimensional coordinates of the targets that were installed on the third concrete beam were measured before and after loading 900 kg.

Point	Before loading (Zero Load)			After loading (900 kg)			Deflection (m)
	X_0 (m)	Y_0 (m)	Z_0 (m)	X_A (m)	Y_A (m)	Z_A (m)	
1	104.4011	102.324	31.533	104.3811	102.32	31.513	0.020
2	104.2012	102.557	31.527	104.1802	102.549	31.505	0.022
3	103.99	102.779	31.522	103.968	102.771	31.499	0.023
4	103.7927	102.994	31.522	103.7687	102.986	31.497	0.025
5	103.588	103.209	31.527	103.585	103.183	31.501	0.026
6	103.463	103.413	31.5247	103.455	103.386	31.4967	0.028
7	103.155	103.62	31.5213	103.152	103.594	31.4953	0.026
8	102.942	103.833	31.5273	102.939	103.807	31.5013	0.026
9	102.7408	104.052	31.53	102.7168	104.044	31.505	0.025
10	102.5402	104.267	31.531	102.5182	104.259	31.508	0.023
11	102.321	104.478	31.522	102.301	104.471	31.501	0.021

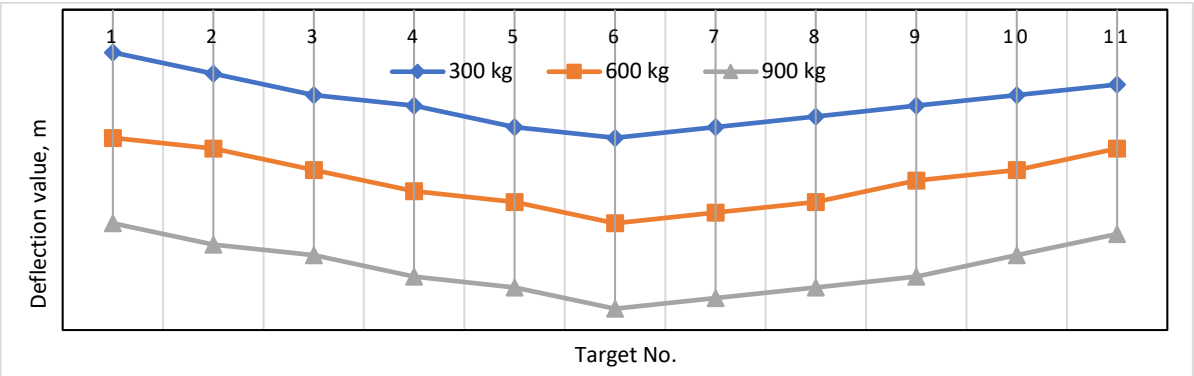

Figure 11. Beam3 deflection under 300 kg, 600 kg, and 900 kg vertical load.

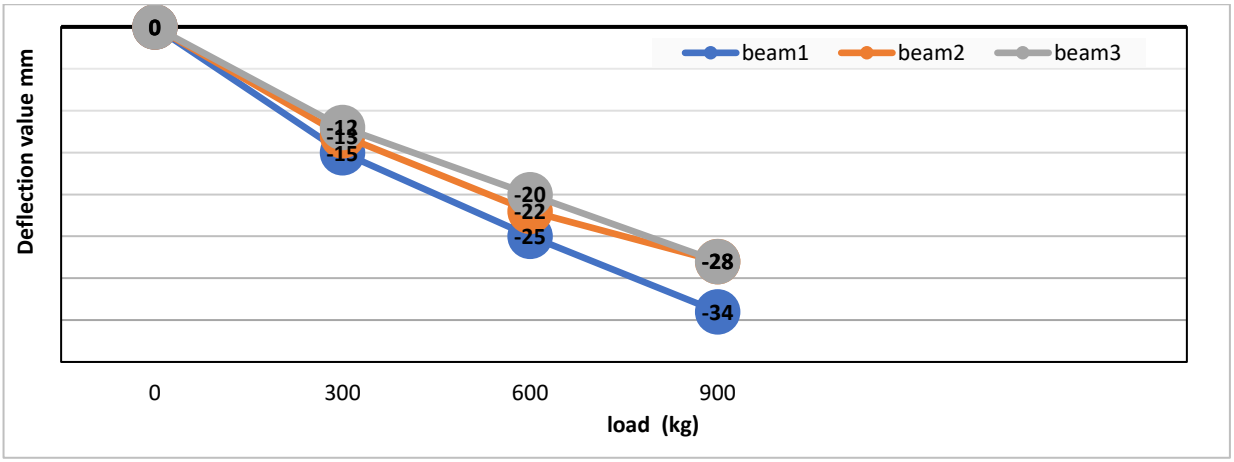

Figure 12. Deflection values in the load area.

4. Conclusions

This study analyses if video measuring and digital cameras can detect concrete beam deformations under pressure. Concrete threshold monitoring and recording are part of the project. The differential load affects concrete beam deflection precision. This study used three 3.20-m-long, 130-by-100-mm-cross-section concrete beams, where three experiments were conducted for three types of concrete beams with the same cross-sectional and longitudinal dimensions. Two low-resolution digital cameras (Canon IXUS 185) were used in these experiments. The research discussed the validation of the results in several steps while observing the dynamic behavior of the concrete beams under vertical loading. The RMS values from the camera calibration process were up to 0.111 pixels. To assess the suitability of video measurement techniques for capturing differences in measurements. Each camera photographed the identical concrete beam three times. It was empty before 300 kg were added. After being laden with 600 kg and 900 kg, there was no burden again. Target site three-dimensional coordinates were obtained using PMS. The RMSE values in the 3D measurements of targets fixed on the steel frame were 0.00313 m, 0.00321 m, and 0.00258 m in the X, Y, and Z coordinates respectively. Thus, the videogrammetric method was used to calculate the 3D coordinates of concrete beam locations before and during load. Deflection values are accurately determined using this method. The obtained deflection values were highly accurate, down to the millimeter level. The study shows the parameter-load correlation. In addition to resistance and cross-sectional properties, video measurement equipment calculates concrete beam deflection. 1) The study compared the photogrammetric triangulation methodology, used for 3D measurement applications, with the accurate conventional method known as Total Station. The results showed that the photo modeler is a reliable tool. Computer programme. 2) The proposed methodology proved that good accuracy can be obtained, by comparing the coordinates observed by the total station with those measured by the videogrammetric system technique. 3) The results provided evidence for the applicability of the Dynamic Videogames methods to assess the concrete beam's structural behaviors and cracks measurement and for the satisfactory level of accuracy of the attained results. This method works well for extensive inspections of critical civil structural elements.

The research discussed the validation of the results in several steps while observing the dynamic behavior of the concrete beams under vertical loading.

References

1. Tong, X, Luan, K, Liu, X, Liu, S, Chen, P, Jin, Y, Lu, W, Huang, B. Tri-Camera High-Speed Videogrammetry for Three-Dimensional Measurement of Laminated Rubber Bearings Based on the Large-Scale Shaking Table. Remote Sensing. 2018. 10(12). Article no. 1902. DOI: 10.3390/rs10121902
2. Galloway, T., Cole, M., & Lewis, C. (2017). Interactions of microplastic debris throughout the marine ecosystem. Journal of Cleaner Production, 169, 41-48. DOI: 10.1016/j.jclepro.2017.05.011.
3. Olsson, K., Pettersson, J. Fatigue Assessment Methods for Reinforced Concrete Bridges in Eurocode: Comparative study of design methods for railway bridges. Master of Science Thesis in the Master's Programme Structural Engineering and Building Performance Design. Chalmers University of Technology. Göteborg, 2010. 167 p.
4. Alaloul, W.S., Qureshi, A.H., Musarat, M.A., Saad, S. Evolution of close-range detection and data acquisition technologies towards automation in construction progress monitoring. Journal of Building Engineering. 2021. 43(3). Article no. 102877. DOI: 10.1016/j.jobe.2021.102877
5. Radi, F.M., Al-Baghdadi, J.A.A. The possibility of using a digital camera and videogrammetric techniques for monitoring of objects moving at different speeds. International Journal of Civil Engineering and Technology. 2018. 9(8). Pp. 318–331.
6. Fathi, H., Brilakis, I. Automated sparse 3D point cloud generation of infrastructure using its distinctive visual features. Advanced Engineering Informatics. 2011. 25(4). Pp. 760–770. DOI: 10.1016/j.aei.2011.06.001

7. Ortiz-Coder, P., Sánchez-Ríos, A. An Integrated Solution for 3D Heritage Modeling Based on Videogrammetry and V-SLAM Technology. Remote Sensing. 2020. 12(9). Article no. 1529. DOI: 10.3390/rs12091529
8. Gruen, A. Fundamentals of videogrammetry – A review. Human Movement Science. 1997. 16(2–3). Pp. 155–187. DOI: 10.1016/S0167-9457(96)00048-6
9. Shi, H., Chen, P., Zhang, D., Yang, J., Xu, Z., Tong, X. High-speed videogrammetric measurement of the displacement of suspendome structure node. Proceedings of The Fifth International Conference on Geoscience and Remote Sensing Mapping (ICGRSM 2023). 2024. 12980. DOI: 10.1117/12.3020958.
10. Maas, H.G., Kersten, T.P. Experiences with a high resolution still video camera in digital photogrammetric applications on a shipyard. Intercongress Symposium. Vol. 30. Part V. Melbourne, 1994. Pp. 250–255.
11. Hu, H., Liang, J., Xiao, Z.Z., Tang, Z.Z., Asundi, A.K., Wang, Y.X. A four-camera videogrammetric system for 3-D motion measurement of deformable object. Optics and Lasers in Engineering. 2012. 50(5). Pp. 800–811. DOI: 10.1016/j.optlaseng.2011.12.011
12. Black, J.T., Pappa, R.S. Photogrammetry and Videogrammetry Methods for Solar Sails and Other Gossamer Structures. Collection of Technical Papers – AIAA/ASME/ASCE/AHS/ASC Structures, Structural Dynamics and Materials Conference 2003. 3. 1–11. DOI: 10.2514/6.2004-1662
13. Whiteman, T., Lichti, D.D., Chandler I. Measurement of deflections in concrete beams by close-range digital photogrammetry. Symposium on Geospatial Theory, Proceedings and Applications. Ottawa, 2002. 9 p.
14. Dai, F., Lu, M. Assessing the Accuracy of Applying Photogrammetry to Take Geometric Measurements on Building Products. Journal of Construction Engineering and Management. 2010. 136(2). Pp. 242–250. DOI: 10.1061/(ASCE)CO.1943-7862.0000114
15. Ji, Y., Chang, C.C. Identification of structural dynamic behavior for continuous system based on videogrammetric technique. Smart Structures and Materials 2006: Smart Structures and Integrated Systems. SPIE, 2006. Pp. 447–458.
16. Ganshkevich, Yu.A., Shikhov, N.S., Stoyantsov, N.M. Estimation of deformations of steel constructions of cranes based on photogrammetry. Journal of Physics: Conference Series. 2021. 1926(1). Article no. 012061. DOI: 10.1088/1742-6596/1926/1/012061
17. Chong, A.K., Al-Baghdadi, J.A.A., Alshadli, D. High definition video cameras for measuring movement of vibrating bridge structure. Int Conf Vib Vibro-acoustics. 2014. 1–10.
18. Chen, X., Davis, J., Slusallek, P. Wide area camera calibration using virtual calibration objects. Proceedings IEEE Conference on Computer Vision and Pattern Recognition. CVPR 2000 (Cat. No.PR00662). Vol. 2. Hilton Head, SC, 2000. Pp. 520–527. DOI: 10.1109/CVPR.2000.854901
19. Qandil, A., Zaid, A.I.O. Considerations in the design and manufacturing of a load cell for measuring dynamic compressive loads. 2015 Power Generation System and Renewable Energy Technologies (PGSRET). Islamabad, 2015. Pp 1–6. DOI: 10.1109/PGSRET.2015.7312209
20. Hastawan, A.F., Haryono, S., Utomo, A.B., Hangga, A., Setiyawan, A., Septiana, R., Hafidz, C.M., Triantino, S.B. Comparison of testing load cell sensor data sampling method based on the variation of time delay. IOP Conference Series: Earth and Environmental Science. 2021. 700(1). Article no. 012018. DOI: 10.1088/1755-1315/700/1/012018

Information about the authors:

Sanarya Sabir,
E-mail: sanaohasan4@gmail.com

Jasim Al-Baghdadi,
E-mail: jasim76@gmail.com

Rana Hamdoon,
E-mail: ranamounjeo@mtu.edu.iq

Received 07.06.2024. Approved after reviewing 02.02.2026. Accepted 03.02.2026.